

# MaRVIn: A Cross-Layer Mixed-Precision RISC-V Framework for DNN Inference, from ISA Extension to Hardware Acceleration

Giorgos Armeniakos , Alexis Maras , Sotirios Xydis ,  
and Dimitrios Soudris , *Member, IEEE*

**Abstract**—The evolution of quantization and mixed-precision techniques has unlocked new possibilities for enhancing the speed and energy efficiency of Neural Networks (NNs). Several recent studies indicate that adapting precision levels across different parameters can maintain accuracy comparable to full-precision models while significantly reducing computational demands. However, existing embedded microprocessors lack sufficient architectural support for efficiently executing mixed-precision NNs, both in terms of ISA extensions and hardware design. This limitation results in inefficiencies such as excessive data packing/unpacking and underutilized arithmetic units, leading to performance bottlenecks. In this work, to address these challenges, we propose novel ISA extensions and the micro-architecture implementation specifically designed to optimize mixed-precision execution, enabling energy-efficient deep learning inference on RISC-V architectures. We introduce *MaRVIn*, a cross-layer hardware-software co-design framework that enhances power efficiency and performance through a combination of hardware improvements, mixed-precision quantization, ISA-level optimizations, and cycle-accurate emulation. At the hardware level, we enhance the ALU with configurable mixed-precision arithmetic (2-, 4-, and 8-bit) for weights and/or activations. To further improve execution efficiency, we employ multi-pumping to reduce execution latency and implement soft SIMD for efficient 2-bit operations. We also extend ISA to support these mixed-precision operations. At the software level, we integrate a pruning-aware fine-tuning method to optimize model compression. Additionally, we introduce a greedy-based design space exploration (DSE) approach to efficiently search for Pareto-optimal mixed-quantized models. Finally, we incorporate voltage scaling to boost the power efficiency of our system. Our extensive experimental evaluation over widely used DNNs and datasets, such as CIFAR10 and ImageNet, demonstrates that our framework can achieve, on average,  $17.6\times$  speedup for less than 1% accuracy loss and outperforms the ISA-agnostic state-of-the-art RISC-V cores, delivering up to 1.8 TOPs/W.

**Index Terms**—Deep Neural Networks, Mixed-precision, RISC-V, ISA Extension, Hardware Optimization, Energy Efficiency

## I. INTRODUCTION

As deep neural networks (DNNs) continue to evolve, their architectures are becoming more sophisticated to achieve higher accuracy in applications such as computer vision, speech processing, and other domains of artificial intelligence [1]. The growing complexity of these models introduces significant computational demands, making it essential

to adopt optimization techniques that balance efficiency and precision. One such widely embraced approach is quantization, which reduces the numerical precision of neural networks — effectively lowering the bit-width required for storage, computation, and data movement [2].

Traditionally, fixed-precision formats have been the standard in both training and inference, ensuring stability and accuracy. However, recent insights reveal that not all neural network operations necessitate the same level of precision. Some computations can tolerate reduced precision without notable degradation in performance, enabling more efficient processing and lower power consumption. This realization has fueled interest in mixed-precision techniques [3], which dynamically adjust the bit-width based on the requirements of different layers or operations within a model. By allocating high precision only where necessary and reducing it elsewhere, mixed-precision quantization can significantly enhance both computational throughput and energy efficiency [4].

Such techniques are particularly valuable for resource-constrained environments, allowing even compact devices to support increasingly complex neural networks. Despite its potential, implementing mixed-precision execution efficiently on general-purpose CPU architectures remains a considerable challenge. Most Instruction Set Architectures (ISAs) provide only limited support, either restricting precision adjustments to coarse-grained levels [5] or relying on inefficient numerical formats that introduce substantial overhead from operand packing and unpacking [6]. Consequently, unlocking the full benefits of mixed-precision computing requires novel hardware-software co-design strategies that co-optimize computational efficiency while minimizing area and energy overheads of data type mismatch. Addressing these challenges is a key focus in modern computer architecture research, as it holds the potential to significantly enhance the performance of DNNs on resource-constrained RISC-V cores.

Despite ongoing efforts in hardware-software co-design [7]–[9], designing DNNs that strike the optimal balance between performance, accuracy, hardware cost, and model size is an intricate multi-objective challenge, especially for resource-constrained systems like TinyML [10]. Optimizing one factor often compromises another—enhancing accuracy may demand more computational resources, while reducing hardware overhead can degrade model quality. Overcoming this requires innovative strategies that tightly integrate algorithmic optimizations with hardware-aware design, pushing the boundaries of what is possible in edge AI. Importantly, realizing the full potential of such hardware modifications also demands

Received 27 March 2025; revised 24 July 2025; accepted 13 September 2025. (*Corresponding Author: Giorgos Armeniakos*)

G. Armeniakos, A. Maras, S. Xydis and D. Soudris are with the School of Electrical and Computer Engineering, National Technical University of Athens, Athens 15780, Greece (e-mail: {armeniakos, amaras, sxydis, dsoudris}@microlab.ntua.gr).

This work is partially supported by EU Horizon research and innovation programme, under project CONVOLVE, grant agreement No 101070374.

a flexible supporting software stack that can effectively map and optimize models for the underlying architecture.

In this work, we introduce *MaRVIn*, a cross-layer hardware-software co-design framework that incorporates an end-to-end flow supporting hardware enhancements, precision-flexible operations, and ISA-level optimizations. Overall, (i) at the logic level, we introduce nine new mixed-precision configurations via ISA extensions, each activating distinct operational *modes* that improve computational efficiency within the modified processor architecture. (ii) At the software level, our framework incorporates a pruning-aware fine-tuning algorithm that reduces model complexity while maintaining high accuracy. This algorithm jointly explores different pruning ratios per layer and mixed-precision quantization schemes, enabling a fine-grained trade-off between accuracy, performance, and resource usage. Lastly, since circuit-level optimizations have been shown to exhibit a synergistic nature with algorithmic and logic enhancements when applied systematically, a) our framework leverages multi-pumping to allow the ALU to operate at twice the baseline frequency, enabling the execution of two operations per cycle, and b) applies a voltage scaling exploration to maximize potential power gains.

Using our framework, we elucidate the impact of a holistic cross-layer co-design exploration that is proven to outperform single-layer techniques [11], on designing and executing DNN models on RISC-V based processors. Our evaluation of more than 2000 mixed-precision DNN models across popular image classification datasets (MNIST, CIFAR-10, ImageNet), demonstrates that our framework, by extending the ISA of a RISC-V Ibex processor with the proposed approach, delivers an average energy efficiency of 720 GOPs/W and up to 1.4 TOPs/W for a lower than 1% top-1 accuracy degradation. In other words, it achieves an average of 17.6 $\times$  speedup compared to the original Ibex architecture. Finally, we show that our framework offers a scalable performance based on a user’s accuracy constraint; thus, with lower quality criteria, the corresponding numbers can increase up to 1.8 TOPs/W (for up to 4.5% accuracy loss), outperforming significantly state-of-the-art approaches.

**Our main contributions in this work can be summarized as follows:**

- 1) We extend the RISC-V ISA with nine instructions, specifically designed to support various hardware optimizations. To validate the new ISA, we implement the proposed micro-architectural modifications within a modified RISC-V-based processor as a proof of concept.
- 2) We propose *MaRVIn*, an automated framework<sup>1</sup> for generating and evaluating mixed-precision DNNs in an end-to-end manner, from PyTorch to netlist. Our framework integrates a pruning mechanism and enables comprehensive evaluation through cycle-accurate RISC-V emulations.
- 3) We systematically analyze trade-offs between accuracy, speedup, and hardware cost, evaluating four widely used DNNs. Our results demonstrate significant energy efficiency gains, outperforming state-of-the-art approaches.

*MaRVIn* extends our preliminary work [12] by leveraging

<sup>1</sup>Our framework is available open-source at <https://github.com/alexmr09/Mixed-precision-Neural-Networks-on-RISC-V-Cores>

TABLE I: Qualitative comparison of related works.

	[13]	[14]	[15]	[16]	[17]	[5]	[18]	[3]	[9]	[19]	Ours
Mixed Prec.	✓	✓	✓	✗	✗	✓	✓	✓	✓	✓	✓
ASIP <sup>1</sup>	✓	✓	✗	✗	✓	✓	✗	✓	✓	✓	✓
Fine-grained	✗	✗	✗	✗	✗	✗	✓	✗	✓	✓	✓
HW-aware train.	✗	✗	✗	✗	✗	✗	✓	✓	✓	✗	✓
HW Optimiz.	✓	✗	✓	✓	✓	✓	✓	✓	✓	✓	✓
Voltage Scaling	✗	✗	✗	✗	✗	✗	✗	✗	✗	✗	✓
Multipumping	✗	✗	✗	✗	✗	✗	✗	✗	✗	✗	✓
Packing	✗	✗	✗	✗	✗	✗	✓	✗	✗	✗	✓

<sup>1</sup>Application-Specific Instruction set Processor

finer-granularity mixed-precision configurations to enhance flexibility and further improve operational efficiency. In addition, greedy-based DSE strategies are introduced to quickly traverse the newly defined design space, and mixed-quantized models are obtained, optimized in multiple layers of abstraction. Interestingly, compared to our previous version [12], our average gains for less than 1% accuracy degradation are 1.53 $\times$  better, achieved with a similarly small increase in area complexity.

## II. BACKGROUND & RELATED WORK

In recent years, research has focused on compression techniques like pruning and quantization [20] to reduce inference time and memory usage of DNNs on edge platforms. Optimized software solutions, including ARM’s CMSIS-NN [21], Google’s GEMMLowp [22], and STMicroelectronics’ X-CUBE-AI [23], along with deployment frameworks such as DORY [24] for RISC-V PULP processors and MCUNet [25], [26], have gained popularity for running Quantized Neural Networks on commercial hardware. Yet, these tools remain largely restricted to 8-bit or higher precision arithmetic, limiting the potential gains of ultra-low-bit quantization.

Because mainstream processors struggle with sub-byte arithmetic, significant research has focused on designing specialized DNN accelerators [6], [16], [27]–[29]. While these accelerators achieve notable speed and efficiency improvements, their practicality is often undermined by poor scalability, large silicon footprint, and high energy consumption. Power consumption typically ranges from hundreds of milliwatts [6], [16], [27] to several watts [28], making them unsuitable for resource-constrained environments. Additionally, their coarse-grained precision and programming complexity limit flexibility, making them less adaptable to diverse workloads.

An alternative approach has been to extend the RISC-V ISA and design custom functional units optimized for sub-byte operations. PULP-NN [2] enhances DNN inference performance by introducing specialized instructions for packing and extracting smaller data vectors, such as 4-bit and 2-bit representations. However, the additional overhead introduced by these casting operations reduces the efficiency gains at lower bit-widths. XpulpNN [5] expands support to 2, 4, and 8-bit SIMD operations but lacks native support for mixed-precision computations.

Recent works [3], [9], [13], [15] have explored mixed-precision arithmetic as a means to optimize accuracy, latency, and memory consumption in resource-limited environments [17]. UNPU [15] implements bit-serial MAC units

with a fixed activation size and weight precision varying between 1 and 16 bits, while [13] extends a RISC-V core with 2- and 4-bit MAC units, along with a custom controller for executing mixed-precision operations across 2, 4, and 8-bit data. Mix-GEMM [3] and SySMOL [9] present co-design methodologies that integrate hardware accelerators with hardware-aware training techniques. However, Mix-GEMM considers only per-network quantization, potentially overlooking finer-grained precision tuning, whereas SySMOL restricts quantization to 1, 2, and 4-bit intra-layer precision, which may lead to accuracy degradation, particularly on complex datasets like ImageNet. Additionally, neither approach leverages low-level optimizations such as clock frequency scaling [30] or the efficient packing of multiple low-precision operations within a single computational block [18] to enhance throughput.

Table I presents a qualitative comparison among key studies on RISC-V ISA extensions for mixed-precision DNNs, summarizing the discussion above. Unlike prior works, *MaRVIn* uniquely introduces mixed-precision instructions that not only enable diverse computation modes but also integrate logic- and circuit-level optimizations, such as multi-pumping and soft SIMD, to enhance efficiency. Furthermore, *MaRVIn* applies hardware-aware fine-tuning to optimize model performance while considering quality constraints, offering an end-to-end framework that spans from ISA extensions to efficient hardware acceleration. To the best of our knowledge, no existing method systematically combines these techniques. In Section V-D, we provide a detailed evaluation against state-of-the-art approaches.

### III. CONFIGURABLE MIXED-PRECISION ARCHITECTURE BASED ON IBEX CORE

The base design in this work leverages Ibex [31], a lightweight and extensible 32-bit RISC-V CPU core (Fig. 1), widely used in energy-efficient and embedded AI applications due to its compact footprint, configurability, and active open-source development. Ibex has been silicon-proven in notable tape-outs, demonstrating its reliability and relevance in real-world deployments. Without loss of generality, the specific RISC-V core serves as a reference microarchitecture scenario to showcase the impact when enabling in an execution unit the support of fine-grained mixed-precision operations, and thus can also be generalized in a straightforward manner to other RISC-V CPU cores [32], [33], with potentially similar area overheads. Note that while micro-architectural modifications are Ibex-specific, our configurable mixed-precision unit and the ISA extensions are RISC-V compliant and core-agnostic.

As shown in Fig. 1, in Ibex, the instruction fetch stage retrieves instructions from memory, which are then passed to the decode and execution stage. Here, the instructions are decoded to determine their operation and operands, and the ALU performs arithmetic/logic operations accordingly. Finally, the results are written back to the register file in the Writeback stage, completing the instruction cycle and enabling subsequent instructions to be executed. The decode logic needs to be enhanced to support newly introduced instructions while also accommodating operations, examining both operands (i.e.,

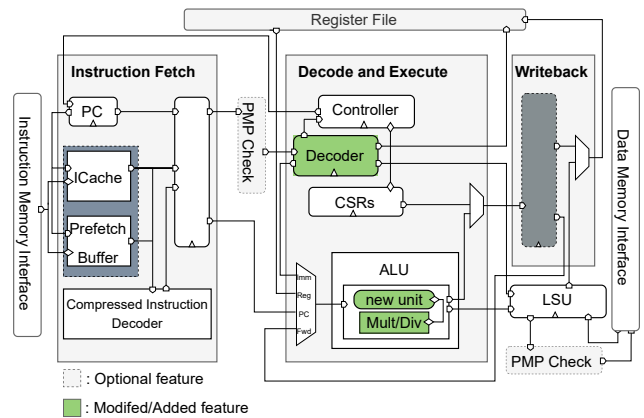


Fig. 1: Ibex core architecture showcasing our modified/added features. Figure obtained from [12].

weights and activations). This enhancement ensures proper signaling to the ALU or any newly added processing unit about the specific operation to execute. The rest of the processor's architecture, including control logic, forwarding mechanisms, and load/store units, remains unchanged.

In the following subsections, we analyze how we modify the ALU unit to support precision-flexible operations (subsection III-A), then how these operations work and are mapped to the different respective *modes* (subsection III-B), and lastly how we incorporate these *modes* into new RISC-V ISA extensions (subsection III-C).

#### A. Configurable Mixed-Precision Unit Design

In this section, we detail our approach to extending the RISC-V CPU core to support fine-grained mixed-precision operations, coupled with hardware optimizations, and thereby improving run-time/energy efficiency, albeit with a small, yet acceptable, degradation in accuracy. Multiple studies have demonstrated the effectiveness of aggressive hardware storage strategies in optimizing arithmetic datapaths [5], [9]. Hence, the key idea is to allow multiple parallel operations (i.e., MAC/MUL units) by leveraging existing logic in architectures such as multiplication units, thereby introducing minimal hardware overheads.

To achieve this, we propose and implement a modified version of Ibex's generic multiplier, expanding its capability to handle variable mixed-precision operations. Since we primarily focus on further optimizing the performance, rather than reducing total area, we firstly select as our baseline unit the one-cycle multiplier (RV32M) [31], featuring three parallel  $17\text{-bit} \times 17\text{-bit}$  multiplication units and a 34-bit accumulator (Fig. 2). Then, we expand this unit within initial ALU by integrating an additional 17-bit multiplier (gray MUL in Fig. 2), allowing for parallel execution of finer-grained mixed-precision multiplications with varying bit-widths. Interestingly, in Ibex's FPGA prototype, the additional 17-bit multiplier accommodates the existing DSPs (i.e., 4 in total) and thus introduces minimal overhead. To perform 32-bit multiplication  $A \times B$  in the Ibex core, the operands are divided into 16-bit



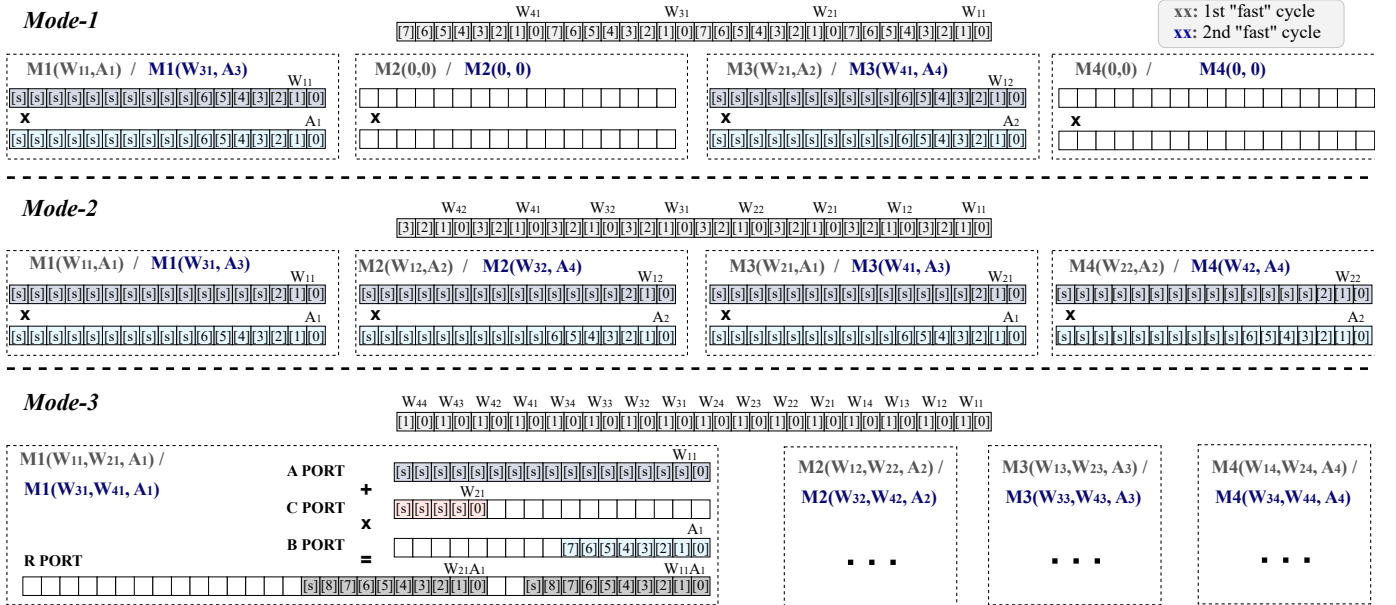


Fig. 3: An illustrative example demonstrating optimized MAC operation and its mapping onto four multipliers (M1, M2, M3, M4), where each multiplier is expressed as a function of the corresponding weights ( $W_{i,j}$ ) and activations ( $A_k$ ). Only a partial load of weights and activations is depicted for simplicity. In *Mode-1*, four 8-bit weights are packed and mapped onto two Mult units ( $M_x$ ) along with their respective activations ( $A_k$ ), with the remaining operations executed in the second fast cycle. In *Mode-2*, eight 4-bit weights are packed and distributed across all four Mult units ( $M_x$ ) over two fast cycles. In *Mode-3*, sixteen 2-bit weights are packed, with each Mult unit ( $M_k$ ) processing two weights per fast cycle alongside the corresponding activations.

store instructions required by the initial (non-scaled) tactic. Moreover, without changing the existing dataflow, the packing of activations creates a higher *input reuse* [34] opportunity. By exploiting the sliding window mechanism, consecutive convolution operations share overlapping input data, minimizing redundant data movement (fewer memory accesses) and improving computational efficiency (reduced cycles per convolution operation).

Also at the logic level, and specifically only when 2-bit operands are used for weights, we apply a **soft SIMD** technique, making full use of the 17-bit multiplier's resources and handling as many MAC operations as possible. An example of this packing technique is shown in Fig. 3c (Mode-3), where 2-bit weights and 8-bit activations are used. Each  $int2 \times int8$  multiplication yields up to a 10-bit result and thus, the second output within the accumulator must start at bit position 11 to prevent any overlap. Additionally, for the accumulations performed in Port R during neuron computations, the required bit width must account for possible overflow when summing multiple values. In our case, using the formula  $w = n + \log_2 k$ , we determine that 2 extra guard bits are needed to safely prevent overflow when accumulating  $k$   $n$ -bit values. Therefore,  $W_{21}$  is shifted by 12 bits (10 bits for the multiplication result plus 2 guard bits) in Port C. Hence, the output is calculated as follows:

$$(A_1) \cdot (W_{21} \cdot 2^{12} + W_{12}) = A_1 W_{21} \cdot 2^{12} + A_1 W_{11} \quad (7)$$

The first product  $A_1 W_{11}$  occupies the 10 least significant bits,

and  $A_1 W_{21}$  is shifted by 12 bits to avoid overlap and ensure accuracy. This design makes efficient use of the accumulator width without additional overhead, as operand placement is automatically handled by the decoder and managed by the arithmetic units.

At the circuit level, motivated by the fact that smaller parallel computing units can achieve higher maximum clock frequencies, we employ **multi-pumping**. Multi-pumping is traditionally employed to reduce resource utilization rather than execution latency [35]. However, in this work, we exploit the fact that some functional units, such as the simpler ALU unit, have shorter critical path delays compared to more complex units. This allows us to run the ALU at twice the core clock speed, effectively executing two operations per core cycle, ensuring both clock domains are phase-aligned and derived from a common PLL, which eliminates the need for asynchronous FIFOs. By applying this technique to low-precision MAC operations, we accelerate the processing of packed operands: in the first *fast* cycle, a subset of partial products is computed, and in the second *fast* cycle, the remaining operations are completed and re-synchronized back to the slow domain through an additional register stage. This ensures a continuous execution flow without additional stalls, while significantly reducing the total cycle count, primarily due to fewer weight and input memory accesses, as further discussed in the following section.

Summarizing, our nine mixed-precision configurations, combined with the previously discussed optimization techniques, can be grouped into three distinct modes. Each mode

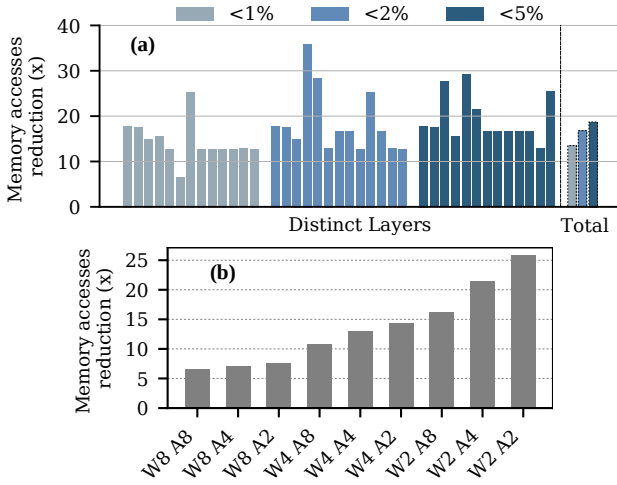


Fig. 4: Memory access reduction compared to the baseline model when mapping mixed-precision operations onto the modified Ibx architecture. (a) Analysis of distinct layers from three mixed-quantized MobileNetV1 models (1%, 2%, 5% accuracy loss). (b) Contribution of each configuration for a single convolutional layer.

supports the same operations but differs in the bit-width of activations, offering precision levels of 2-bit, 4-bit, and 8-bit:

- 1) *Mode-1* (low-speed): if 8-bit precision is used for weights (Fig. 3a), then multi-pumping has zero impact, since only 4 weights are loaded in one 32-bit register during the first iteration. Speedup is accomplished only due to multipliers parallelization and **data packing**.
- 2) *Mode-2* (medium-speed): if 4-bit precision is used for weights (Fig. 3b), both **multi-pumping** and data packing contribute to processing acceleration.
- 3) *Mode-3* (high-speed): if 2-bit precision is used for weights (Fig. 3c), our third **soft SIMD** optimization technique is also applied. In other words, *Mode-3* is an optimized derivative of *Mode-2*.

### C. RISC-V ISA Extension

To illustrate the speedup of our *modes*, we extend the RISC-V ISA to support nine different operations, following the RISC-V ISA manual for custom extensions. Each set of three instructions corresponds to a single mode, defined by weight and activation bit-widths, resulting in three modes and a total of nine configurations. These nine instructions use the R-type format with six sub-fields: opcode, func3, func7, rs1, rs2, and rd, all 32 bits long. The opcode specifies the operation and the involved source (rs1, rs2) and destination (rd) registers. Func3 and func7 define the operations based on the input format.

Our RISC-V mixed-precision extension instructions are listed in Table II. We introduce only a few instructions, having no impact on the CPU’s opcode decoder hardware. As an example, *nn\_mac\_w8a8* corresponds to *Mode-1* and requires four 8-bit packed weights and four 8-bit activations for four parallel MAC operations. *nn\_mac\_w4a4* and *nn\_mac\_w2a4* correspond to *Mode-2* and *Mode-3*, requiring eight 4-bit and 16 2-bit packed weights, respectively, with eight 4-bit activations. In all cases, the accumulator (rd) length is 32 bits.

TABLE II: Overview of the mixed-precision ISA extension encoding.

	func7	func3	rs1 (A)	rs2 (W)	rd (Acc)	Description
<i>nn_mac_w8a8</i>	000 1010	010	4 8-bit	4 8-bit	32-bit	Mode-1
<i>nn_mac_w8a4</i>	000 0110	010	8 4-bit	4 8-bit	32-bit	Mode-1
<i>nn_mac_w8a2</i>	000 0010	010	16 2-bit	4 8-bit	32-bit	Mode-1
<i>nn_mac_w4a8</i>	000 1001	010	4 8-bit	8 4-bit	32-bit	Mode-2
<i>nn_mac_w4a4</i>	000 0101	010	8 4-bit	8 4-bit	32-bit	Mode-2
<i>nn_mac_w4a2</i>	000 0001	010	16 2-bit	8 4-bit	32-bit	Mode-2
<i>nn_mac_w2a8</i>	000 1000	010	4 8-bit	16 2-bit	32-bit	Mode-3
<i>nn_mac_w2a4</i>	000 0100	010	8 4-bit	16 2-bit	32-bit	Mode-3
<i>nn_mac_w2a2</i>	000 0000	010	16 2-bit	16 2-bit	32-bit	Mode-3

After completing the MAC operations for each output feature, Ibx’s standard dataflow is executed: results are retrieved from the 32-bit accumulators, followed by a requantization step to adjust the output bit-width back to 8 bits.

The key takeaways of our introduced instructions for enabling different operational *Modes* are twofold. Firstly, they facilitate a higher number of multiply operations per cycle (as shown in Section III-B), leading to increased throughput. Secondly, they significantly reduce the number of loads and stores, leading to fewer memory accesses, as parameters are packed and more data can be fetched in a single transfer.

For example, the reduction in memory accesses per layer (13 in total) for MobileNetV1 is depicted in Fig.4a. To generate Fig.4a, we examined three mixed-precision models, ranging from high-quality models (<1% accuracy loss) to less-quality ones (up to 5%), and obtained memory accesses from Verilator [36], by reporting control status of all registers. This systematic exploration is detailed in Section IV. As illustrated, even with minimal quality degradation, memory accesses across different layers are reduced in total from  $13.5\times$  up to almost  $19\times$ . In Fig. 4b, a deeper analysis is provided for a single convolutional layer, highlighting the impact of setting different bit-widths for weights and activations across all MAC operations within the same layer. Depending on the various mixed-precision configurations, the memory access reduction is shown to range from  $6.5\times$  to nearly  $26\times$  when aggressive precision (*W2A2*) is applied. Part of this reduction also stems from fewer pipeline stalls caused by weight/input fetches and data hazards, which account for roughly 30% of the total execution cycles.

**Compiler support:** Once the encoding of the instructions has been done, we provide a high-level interface for their integration. Our approach involves implementing a C intrinsic for each instruction, utilizing the inline assembly `__asm__` operator to emit the bytecode corresponding to the specific instruction. These instructions are then inserted automatically by our framework according to the model’s mixed-precision configurations. An example with detailed instruction formats in both a baseline version and an optimized one is provided in Listings 1 and 2, respectively. This approach prevents us from integrating code generation within the compiler. To facilitate the inline assembly support for our custom instructions, we made minor adjustments to the RISC-V GNU toolchain within GCC’s binutils. This modification enables the execution of any

RISC-V binary on various architectures (e.g., x86 of a host machine). Finally, the compiled binaries, along with the complete instruction set containing all our extensions, are executed and thoroughly emulated using the Spike simulator [37].

```
for (int i = 0; i < num_outputs; i++)
  for (int j = 0; j < num_inputs; j++)
    out[i] += w[i][j] * a[j];
```

Listing 1: Baseline matrix-vector multiplication in C.

```
for (int i = 0; i < num_outputs/4; i++)
  for (int j = 0; j < num_inputs/4; j++)
    asm volatile("nn_mac_w8a8 %0,%1,%2\n":
      "=r"(out[i]):"r"(a[j]),
      "r"(w[i][4*j]));
  ...
  asm volatile("nn_mac_w8a8 %0,%1,%2\n":
    "=r"(out[i]):"r"(a[j]),
    "r"(w[i][4*j+3]));
```

Listing 2: Matrix-vector multiplication with custom ISA. Bold letters highlight vectorized variables, indicating that they contain compressed elements. Each variable holds four 8-bit values, i.e.,  $\text{out}[i] = \{\text{out}[4i], \text{out}[4i+1], \text{out}[4i+2], \text{out}[4i+3]\}$ .

#### IV. UNIFIED FRAMEWORK FOR CROSS-LAYER CO-DESIGN EXPLORATION

This section outlines the workflow of our automated framework (Fig. 5) for generating mixed-precision neural networks and evaluating their performance on RISC-V CPU cores. This workflow extends our preliminary version [12] with three key improvements: i) an enhanced DSE, incorporating the pruning technique, ii) support for nine new instructions, and iii) the introduction of voltage scaling exploration to boost power efficiency.

Briefly, our framework (Fig. 5) receives as input a trained model (e.g., dumped from PyTorch) and performs a two-stage exploration process at the software and then at the circuit level. At the software level, the framework systematically explores various model configurations by first applying PyTorch’s native structural pruning method to examine different percentages of connections to prune per layer. Following this, it evaluates fine-grained mixed-precision configurations for each layer, considering 2-bit, 4-bit, and 8-bit precision for both weights and activations. Once the final Pareto-optimal models are identified, logic-level optimizations are implemented by mapping operations to various operational modes based on their precision configurations. Subsequently, the framework transitions to circuit-level exploration, applying voltage scaling to evaluate trade-offs among operating voltage, power consumption, and system frequency. This stage also explores the available slack time and investigates how the multi-pumping technique can be fully exploited, enabling maximum potential power gains at the same time.

Once the functionality of the **nine** new instructions is simulated and verified, the linker generates a single executable file (ELF). This file, along with the RTL descriptions of the modified core—written in SystemVerilog and synthesized using industry-standard EDA tools (Xilinx Vivado for FPGA flow and Synopsys Design Compiler for ASIC flow)—is provided as input to Verilator [36], a cycle-accurate emulator.

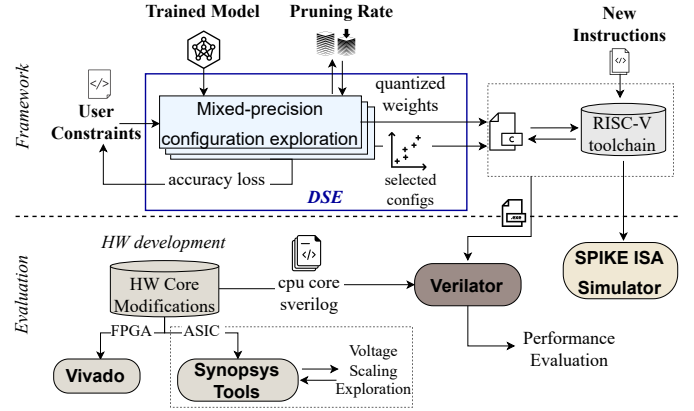


Fig. 5: Overview of our proposed framework flow diagram

The flow reaches the synthesis stage, but post-layout PnR validation is not performed in this flow. Additionally, we apply voltage scaling using Synopsys tools under different operating conditions. This setup allows for a comprehensive evaluation of performance metrics, including accuracy-speedup trade-offs, power consumption, and any introduced overheads.

##### A. Mixed-precision exploration

One of our primary objectives in our work, as well as a key challenge in multi-objective optimization co-design approaches, is to identify, quite fast, a close-to-optimal design solution. To tackle this challenge, we adopt a greedy search method (Algorithm 1). Note that while greedy algorithms have been proven to extract good enough solutions in complex optimization problems [38], any other algorithms (such as heuristics [16]) can be seamlessly employed.

Our mixed-precision DSE starts with a pre-trained model  $m$ , where we systematically adjust different pruning rates and precision settings, which allow us to identify configurations that balance computational efficiency along with a user’s user-defined accuracy loss threshold  $T$ . The process begins by iterating over a range of pruning rates, defined in steps of a granularity parameter  $g$ , up to a maximum pruning rate  $p_{max}$ . The pruning rate is simply defined as the percentage of weights per layer that are set to zero during the pruning-aware post-training process. For each pruning rate, we analyze the impact of mixed-precision configurations on the latency of each layer in the model (line 3). Specifically, we evaluate all possible configurations per layer (e.g., 2-bit, 4-bit, and 8-bit precision for weights and activations) and select an arbitrary medium-latency configuration  $C_l$  (line 7) for each layer as a starting point set  $C_{start}$  (line 9). The latency of each layer can be quickly estimated using Verilator, without executing the entire model. This enables us to narrow down the design space and avoid exhaustive evaluation of all possible configurations. The initial setting, consisting of medium-latency configurations for all layers, is then evaluated for accuracy (line 10). If the accuracy of this starting point remains within the acceptable threshold (i.e., the accuracy loss does not exceed  $T$ ), a full DSE is triggered (line 12). During this exploration, all remaining combinations of precision configurations are evaluated,

**Algorithm 1** Pseudocode for Mixed-Precision DSE

---

**Input:** 1) Pretrained Model  $m$ , 2) Accuracy Loss Threshold  $T$ ,  
3) Granularity  $g$ , 4) Max Pruning Rate  $p_{\max}$ , 5) Iterations  $I$  for DSE  
**Output:** Design space  $\mathcal{D}^*$  with acceptable mixed-precision configurations

```

1: for  $p \in \{0, g, 2g, \dots, p_{\max}\}$   $\triangleright$  Iterate over pruning rates
2:   for each layer  $l \in m$ 
3:     Calculate latency for all (9) configurations of  $l$ 
4:   end for
5: end for
6: for each layer  $l \in m$ 
7:    $C_l \leftarrow$  medium latency config
8: end for
9:  $C_{\text{start}} \leftarrow \{C_l \mid l \in m\}$   $\triangleright$  A set of  $C_l$  instances as starting point
10: Evaluate accuracy  $\mathcal{A}_{\text{start}}$  of  $C_{\text{start}}$ 
11: if  $\mathcal{A}_{\text{start}} \geq \mathcal{A}_m - T$   $\triangleright$  Check accuracy constraint
12:   Perform full design space exploration:
      $\mathcal{D} = \bigcup_{l \in m} \{C_l \mid \text{remaining combinations}\}$ 
     Discard higher precision configs:
      $\mathcal{D} \leftarrow \mathcal{D} \setminus \{C_l \mid b_w, b_a \text{ are higher than current settings}\}$ 
     until DSE reaches  $I$  iterations, terminate process
13: else
14:    $l_{\min} \leftarrow \arg \min_{l \in m} \text{compute\_intensity}(l)$ 
15:   Move to a higher configuration for  $l_{\min}$ :
16:    $C_l \leftarrow C_l^{\text{higher}} \mid \text{latency}(C_l^{\text{higher}}) > \text{latency}(C_l)$ 
17:   if  $\mathcal{A}_{\text{new}} \geq \mathcal{A}_m - T$   $\triangleright$  Check accuracy constraint
18:     Perform full design space exploration:
        $\mathcal{D} = \bigcup_{l \in m} \{C_l \mid \text{remaining combinations}\}$ 
        $\mathcal{D} \leftarrow \mathcal{D} \setminus \{C_l \mid b_w, b_a \text{ are higher than current settings}\}$ 
       until DSE reaches  $I$  iterations, terminate process
19:   else
20:     Go to step 15
21:   end if
22: end if
23: return  $\mathcal{D}$ 

```

---

excluding those with higher precision settings than the current configuration. By pruning these higher precision configurations, we can reduce the search space and focus on solutions with lower computational costs. If the accuracy constraint is not satisfied with the initial configuration, the algorithm identifies the layer with the lowest computational intensity in terms of required cycles and incrementally adjusts its precision to a higher setting (line 15). This iterative process ensures that only the necessary adjustments are made to meet the accuracy threshold while minimizing computational overhead. After each adjustment, the model's accuracy is re-evaluated, and the process is repeated until the accuracy constraint is satisfied or all layers have been adjusted to their maximum allowable precision. The entire process is terminated when DSE reaches  $I$  iterations (line 12 or line 18), an arbitrary number set by the user, to control iterations and prune the design space, ensuring no strict omissions of combinations between layers and configurations. Subsequently, a set  $\mathcal{D}$  of acceptable mixed-precision configurations is returned (line 23).

Moreover, based on our experiments, the proposed greedy-based exploration consistently identifies solutions close to optimal. For example, in the case of LeNet, our hypervolume analysis [39] shows that it covers 73% of the optimal trade-off space (as defined by exhaustive DSE), while achieving this with  $14\times$  less runtime. This highlights both the scalability and the practical relevance of our method, particularly for larger models where exhaustive search is infeasible.

Finally, given a selected mixed-precision configuration among the obtained Pareto space, our framework evaluates

the model as follows:

- 1) Obtains from the user the C source code, which includes the respective replacements of the original kernels with kernels incorporating the  $mn\_mac\_w[x]a[y]$  operations.
- 2) Updates the RISC-V toolchain with the new instructions, verifies their functionality in the Spike simulator, and generates the ELF executable file.
- 3) Synthesizes the modified core using EDA tools for FPGA and ASIC technology, and extracts the RTL descriptions.
- 4) Simulates the ISA-extended Ibex processor using Verilator, and, along with Synopsys PrimeTime, extracts performance metrics and power analysis.

Note that only step 1 and 4 need to be executed for different benchmarks or configurations, while steps 2 and 3 are executed only once. Finally, our framework can support any DNN architecture composed of layers currently covered by our implemented kernels, including depthwise convolutional layers, dense layers, residual blocks, and pooling layers.<sup>2</sup>

### B. Voltage-scaling exploration

To evaluate the impact of voltage scaling on our modified Ibex system, which integrates both the core and accelerator, we conducted a comprehensive power-performance analysis. The design was synthesized at a 250 MHz clock frequency, and this process ensured accurate characterization through Composite Current Source (CCS) models, under typical conditions (TT, 25°C) at 0.8V. The synthesized netlist underwent functional validation in Siemens QuestaSim 2024.3, generating VCD files later converted to SAIF for power estimation. For voltage scaling exploration, we employed a Unified Power Format (UPF) description to define power domains, voltage levels, and retention strategies, ensuring correct functionality across multiple voltage conditions. Using PrimeTime, we conducted timing and power analysis at different voltage corners through *define\_scaling\_lib\_group*, considering standard cell characterizations from 0.6V to 1.0V while maintaining constant temperature conditions. By sweeping voltage levels in 0.05V increments, we systematically analyzed power consumption and performance (GOPs/W) without extrapolation.

The results show that lowering the supply voltage significantly reduces power consumption while maintaining a constant operating frequency, leading to improved energy efficiency (GOPs/W). The total power dissipation of a circuit is given by:

$$P_{\text{total}} = P_{\text{static}} + a \times C \times f_s \times V_{dd}^2, \quad (8)$$

where  $a$  is the switching activity,  $C$  is the circuit's capacitance,  $f_s$  is the operating clock frequency and  $V_{dd}$  is the supply voltage. Since dynamic power scales quadratically with  $V_{dd}$  and static power also decreases at lower voltages, power dissipation is significantly reduced without affecting computational throughput. However, excessive voltage scaling increases timing slack, potentially compromising system stability in more aggressive operating conditions. In our case, instability occurs when the supply voltage drops below 650 mV.

<sup>2</sup>For more details see 'How to test a new model' section at <https://github.com/alexmr09/Mixed-precision-Neural-Networks-on-RISC-V-Cores>

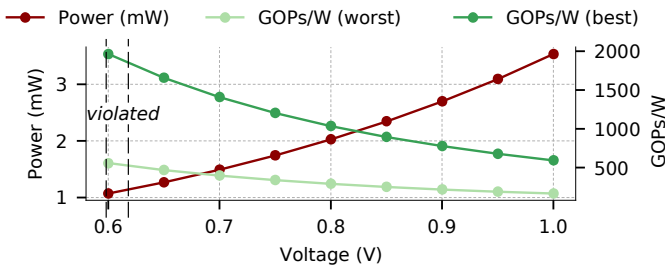


Fig. 6: Impact of voltage scaling on power and energy efficiency in the modified Ibex system through EDA tools. Worst and best cases correspond to applying *W8A8* and *W2A2*, respectively, for the entire model.

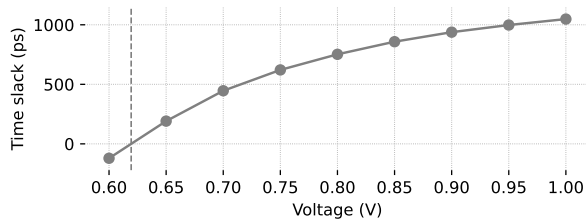


Fig. 7: Time slack versus voltage for the baseline core at 250MHz, showing positive slack above 0.62V and negative slack indicating timing violations below this threshold.

In Fig. 6, we evaluate the impact of voltage scaling on power consumption and energy efficiency. In this figure, we analyze the power dissipation and GOPs/W across different supply voltages ranging from 0.6V to 1.0V. As expected, reducing the supply voltage leads to a quadratic reduction in dynamic power. For instance, by lowering the voltage from 1.0V to 0.7V, power consumption decreases significantly, with a reduction of approximately 58%. This translates directly to a  $2.4\times$  increase in GOPs/W for both the worst and best cases, where the highest configuration (*W8A8*) and the lowest configuration (*W2A2*) are used for the entire inference, respectively. This means that the system operates more efficiently in terms of computational performance per watt. The trend continues as we further scale voltage down to 0.6V, where the lowest power levels are observed. However, as shown in Fig. 7, excessive voltage scaling introduces timing margin violations. Specifically, time slack on the critical path reduces from +1048ps at 1.00V to -121ps at 0.60V, indicating that timing requirements at 250MHz are no longer met below 0.62V. The overall impact of complete model executions with various mixed-precision configurations is evaluated in Section V-D.

## V. EVALUATION & RESULTS

### A. Experimental Setup

In this section, we evaluate the efficiency of *MaRVIn* by performing an in-depth evaluation over four state-of-the-art DNNs trained on four simple and challenging image classification datasets (Table III). For our analysis, we consider: LeNet5, a CNN with 3 convolutional layers [21], MCUNet [25], MobileNetV1 [40], and ResNet18 [41] trained on MNIST,

TABLE III: Description of our evaluated baseline models

Model	Acc (%)	Topology <sup>1</sup>	#cycles	#MAC
CNN (CIFAR10)	78.9	3C-1D	110.9M	12.3M
LeNet5	98.2	2C-3D	7.4M	423K
Mcunet-vww1	88.9	1C-15R-1D	175.6M	12M
MobileNetV1	70.4	14C-1D	5.7B	573M
ResNet18	73.3	17C-1D	18.4B	1.8B

<sup>1</sup>Network’s topology in terms of convolutional (C), dense (D), and residuals (R) layers

CIFAR10, Visual Wake Words [42] and ImageNet dataset, respectively. Our mixed-precision post-training quantization is based on PyTorch libraries and considers 10% of the training dataset, while the fine-tuning process with quantization-aware training is executed using a larger portion of the same dataset and for 25 epochs (with the ability to leverage early stopping if convergence is reached sooner), on average, requiring less than 15 hours each, on an NVIDIA Tesla V100 with 32GB RAM.

For hardware results, we evaluate both ASIC and FPGA synthesis flows (Table IV) for the microarchitecture of the open-source Ibex core [31], described in System Verilog. For the FPGA workflow, we consider a Virtex-7 FPGA as a proof-of-concept platform, with the main core operating at 50MHz and the custom functional unit running at 100 MHz, and used Vivado 2023.1 for synthesis results. The register file is implemented using RAM32M primitives. Cycle-accurate simulations for both performance metrics and top-1 classification accuracy are performed using Verilator [36], which reads Ibex performance counters for a precise report of total cycles. On the other hand, for the ASIC workflow, the processor is implemented in System Verilog RTL and synthesized with a dual-clock configuration, running at 250 MHz for the main core and 500 MHz for the functional unit. The design is mapped to the industrial-strength GlobalFoundries 22nm library, aligning with state-of-the-art approaches. Synthesis is performed using Synopsys Design Compiler with the *compile\_ultra* command, while the register file is implemented using latches. Power analysis is conducted by leveraging the switching activity extracted from the VCD file, combined with the design’s synthesized netlist, enabling accurate power estimation.

### B. DSE Evaluation - Latency vs Network accuracy

As mentioned, our framework starts with a design space exploration to find different mixed-precision configurations and pruning variations for each input model. Fig. 8 presents the Pareto space between accuracy and required number of clock cycles for all the DNNs examined. These clock cycles correspond to the end-to-end execution of the entire network. In Fig. 8, the black star represents the pre-trained baseline model. The gray circles are the quantized models with mixed precision among their conventional or pruned layers, while the green squares form the Pareto front. The blue circles are the Pareto front of our previous version [12], i.e., without adapting the bit-width of activation and without incorporating our pruning approach. This evaluation also includes the minor

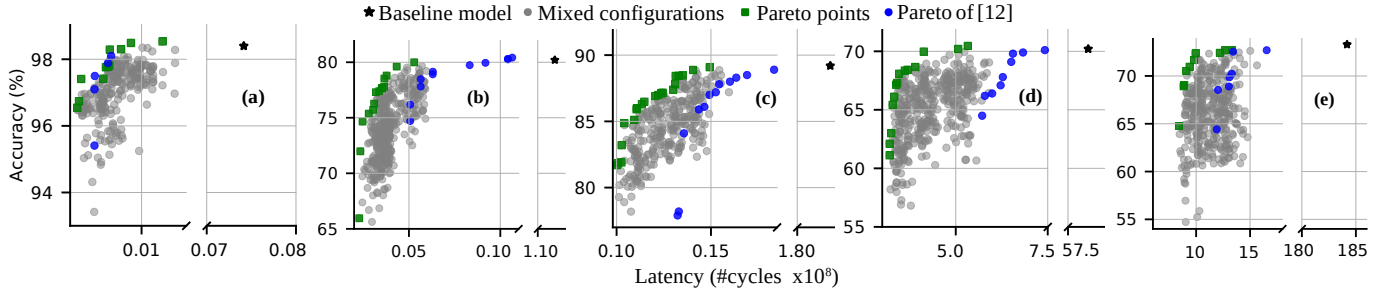


Fig. 8: Pareto Space of accuracy versus latency in clock cycles, obtained from our mixed-precision configuration exploration for LeNet(a), CNN\_CIFAR10(b), MCUNet(c), MobileNetV1(d) and ResNet18(e).

TABLE IV: Performance comparison of our modified Ibox processor with the baseline. The best model per benchmark with less than 1% accuracy loss is considered.

Platform	FPGA		ASIC GF22nm	
	Baseline Ibox	Modified Ibox	Baseline Ibox	Modified Ibox
Clock Freq.	50MHz	50 <sup>1</sup> 100MHz	250MHz	250 <sup>1</sup> 500MHz
Precision	32-bit	2-/4-/8-b	32-bit	2-/4-/8-b
Power (mW)	256 <sup>2</sup>	260 <sup>2</sup>	1.23 <sup>3</sup>	2.03 <sup>3</sup> /1.15 <sup>4</sup>
Resources/ Area	5.5K FF 5.1K LUTs 4 DSPs	7.3K FF 6.2K LUTs 4 DSPs	6616 $\mu$ m <sup>2</sup>	8683 $\mu$ m <sup>2</sup>
Energy Efficiency (GOP/s/W)	LeNet: 0.022 CNN: 0.043 MCUNet: 0.026 MbNetV1: 0.04 ResNet18: 0.038	0.438 1.09 0.34 0.565 0.538	23.1 45.2 26.8 40.9 40	280 <sup>3</sup> / 496 <sup>4</sup> 831 <sup>3</sup> / 1471 <sup>4</sup> 237 <sup>3</sup> / 385 <sup>4</sup> 362 <sup>3</sup> / 639 <sup>4</sup> 344 <sup>3</sup> / 609 <sup>4</sup>

<sup>1</sup>Basic core's clock frequency / Multi-pumped units' clock frequency <sup>2</sup> 28% static power <sup>3</sup> 0.8V operating voltage <sup>4</sup> 0.62V operating voltage

latency overheads (ranging from 0.003% to 1.6% of the total execution cycles) introduced by the pre-processing and operand packing performed at the C level. These steps are fully automated, executed offline, and required only once per model. Note that, compared to our prior version, we integrate Verilator into the DSE to accurately measure cycle counts instead of relying on the number of MAC operations. This adjustment is necessary because determining latency-optimal configurations per layer becomes now a non-trivial problem for our current design space, due to the expanded mixed-precision options (e.g.,  $W8A2$  vs  $W4A4$ ) and varying pruning rates. Furthermore, for the DSE of all models, we set a 1% accuracy constraint, a maximum pruning rate of  $p_{\max} = 50\%$ , and a total of  $I = 500$  iterations. As derived, the number of models explored depends on the number of layers. In total, to generate Fig. 8, we evaluated more than 2000 quantized models. It is observed that different precisions in layers ranging between 2,4 and 8 bits can achieve accuracies comparable to or the same as the full-precision counterparts.

For all benchmarks, more than 92% reduction in the number of cycle counts can be achieved in their mixed quantized

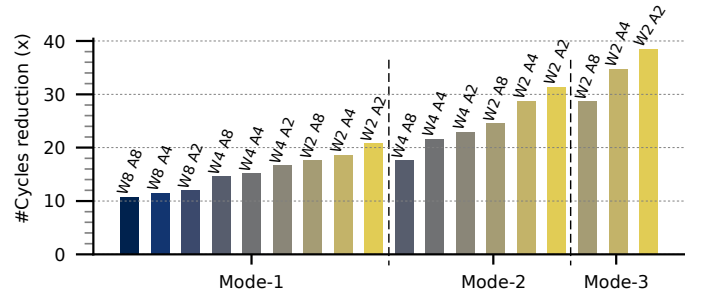


Fig. 9: Cycle count reduction for a convolution layer when using each *Mode*, compared to the baseline. The impact of individual mixed-precision configurations, corresponding to a single optimization per *Mode*, is illustrated.

derivatives for less than 1% accuracy loss, while this number increases to 95% when up to 5% accuracy loss is applicable. Moreover, compared to [12], our enhanced exploration can achieve much better performance, since for less than 1% accuracy loss, the inference time is almost 32% better, on average for all models.

### C. Per-technique analysis

The impact of each distinct optimization technique (different *Mode*) that is applied within a processor execution is evaluated in Fig. 9. To generate Fig. 9 we consider as an example one distinct convolutional layer, i.e., the second layer of the CIFAR10 CNN, and evaluate the relative speedups of the standalone *Mode-1,-2,-3*, in terms of number of cycles reduction. In other words, we report the gains of each technique as if it was solely applied throughout the whole layer and examined for all the nine different bit-widths. As can be noticed, not every single *mode* supports all nine mixed-precision configurations. It is observed that *Mode-1*, due to the high parallelization of 8-bit operands and minimization of loads and stores, can achieve on average  $14\times$  speedup compared to the baseline RV32IMC, and almost  $21\times$  when 2-bit weights and activations are utilized. On the other hand, when the standalone multi-pumping technique is applied (*Mode-2*), it can increase the average speedup to  $24\times$ . Finally, when 2-bit weights are considered (*Mode-3*), our soft SIMD approach obtains an extra speedup, having a significant reduction in total cycles of almost  $34\times$ . Note that this number is increased by

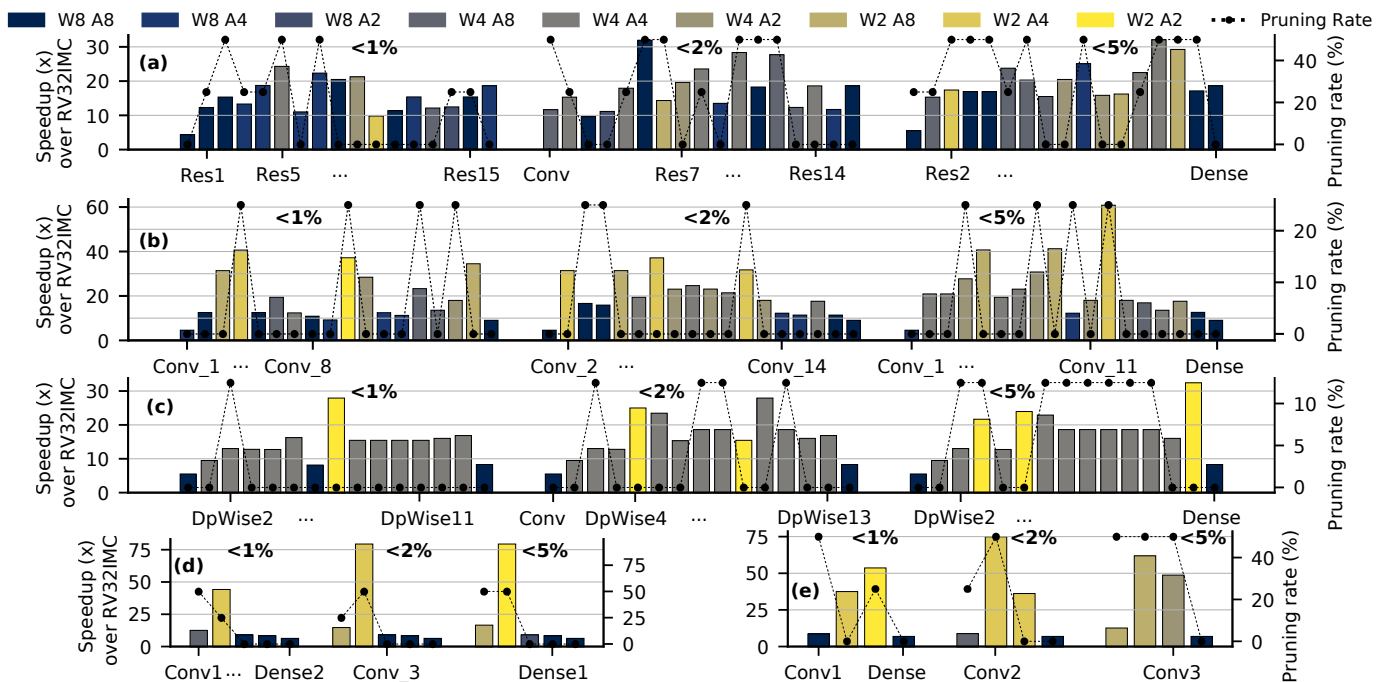


Fig. 10: Speedup gains compared to the baseline Ixex RV32IMC for 4 different benchmarks, i.e., MCUNet (a), ResNet18 (b), MobileNetV1 (c), CIFAR10 CNN (d), LeNet (e), are shown. For each benchmark, three different mixed-precision models have been selected, each one satisfying a different accuracy loss (1%, 2%, 5%). The selected pruning rate per layer, expressed as a percentage, is depicted on the right Y-axis.

$3\times$  compared to our previous work [12], where the bit-width of activations was kept fixed.

Despite the significant speedups, each mode introduces some area and power overhead on top of its previous mode. Specifically, to support mode-1, the modified core introduces a 22% power overhead over the baseline (1.23mW), primarily due to added parallelism. Mode-2 incurs the highest power increase (25% on top of mode-1) because of the multi-pumping technique that doubles the ALU frequency, while mode-3 and soft SIMD add an additional 7%. In terms of area, mode-1 introduces the largest overhead (19%) due to extra logic, while mode-2 and mode-3 add just 4% and 5%, respectively, as they rely mainly on algorithmic techniques. Regarding the FPGA design, mode-1 increases area by 26% in LUTs and 11% in FFs. Mode-2 adds 2% LUTs and 6% FFs over mode-1, while mode-3 contributes an additional 9% LUTs and 2% FFs. DSP usage remains constant across all modes. The total cumulative overheads can be shown in Table IV.

As mentioned earlier, the sensitivity and error resilience of each layer can vary, and hence the top-1 models' accuracy is tightly dependent on the selected precision for each layer. Subsequently, in order to put the delivered trade-offs between total execution time of DNN inference and top-1 accuracy into perspective, and analyze the contribution of each layer and each configuration, we generate Fig. 10. This figure evaluates three user-defined accuracy loss thresholds and extracts corresponding latency-optimal mixed-precision configurations from the DSE, each minimizing latency for its respective accuracy constraint. The bit-width configurations of weights

and activations per layer are depicted using distinct colors, while the right Y-axis shows the pruning ratio for each layer. Then, the speedup for all layers derived from Verilator is reported. The key observations regarding the mixed precision selection are two: 1) the less complex models like LeNet and CIFAR10 CNN allow aggressive quantization down to 2 bits (especially in weights) in most of their layers with minimal accuracy degradation ( $< 1\%$ ) and thus able to achieve the maximum possible performance gains, and 2) although the more challenging MobileNetV1, ResNet18 and MCUNet models barely utilize the beneficial W2A2 configuration, they manage to map most of their layers to W4A4 option with small impact on their accuracy ( $< 2\%$ ). Overall and on average for all layers, our proposed ISA extensions can achieve from  $17.6\times$  up to  $23.3\times$  speedup for 1% up to 5% accuracy degradation, respectively. It is also noteworthy that MCUNet presents less significant gains compared to other benchmarks due to the high amount of depthwise convolutions. The latter do not enable the same degree of data reuse as in standard & point-wise convolutions, while also they differ in the overheads (e.g., branch instructions) they introduce. Finally, these consistent performance gains indicate that our proposed framework could scale effectively from simple models to more complex ones, as it leverages 2-, 4-, and 8-bit precision, which has been shown to preserve high inference accuracy even in larger architectures [4].

#### D. Comparison against state-of-the-art

In this section, we evaluate *MaRVIn* against the most relevant state-of-the-art solutions and our previous version,

TABLE V: Comparison with state-of-the-art solutions. Performance metrics along with precision configurations are presented. Efficiency reflects the raw performance of a typical convolutional layer, using only our least efficient to most efficient mode.

		TC'24 [17]	HPCA'23 [3]	ISVLSI'20 [13]	JSSC'18 [15]	TCAD'20 [16]	DATE'20 [5]	TVLSI'24 [19]	ICCAD'24 [12]	<i>MaRVIn</i>
Architecture	Platform	90nm	22nm	22nm	65nm	65nm	22nm	28nm	7nm	22nm
	Precision	32 b W/A	2-8 b W/A	2/4/8 b W/A	1-16 b W	16 b W/A	2/4/8 b W/A	4/8/16 W/A	2/4/8 b W	2/4/8 b W/A
	Clk Freq.	100MHz	1.2GHz	250MHz	200MHz	200MHz	600MHz	1.05GHz	250MHz	250MHz
	Area/Power	6.44mm <sup>2</sup> / 5.8mW	0.014mm <sup>2</sup> / 9.9mW <sup>3</sup>	0.002mm <sup>2</sup> / 5.5mW <sup>3</sup>	16mm <sup>2</sup> / 288mW	11.47mm <sup>2</sup> / 805mW	0.04mm <sup>2</sup> / 43.5mW <sup>3</sup>	1.20mm <sup>2</sup> / 533mW	0.038mm <sup>2</sup> / 0.58mW	0.009mm <sup>2</sup> / 1.15mW
Performance	GOPs	0.23	11.9	3.3	514	288	47.9	343.1-737.9	0.24-0.85	0.6-2.1
	Area Eff. (GOPs/mm <sup>2</sup> )	0.04	850	1650	32.1	25.1	1198	285.8-614.6	6.3-22.4	66.7-233.3
	Energy Eff. (GOPs/W)	38.8 <sup>1</sup>	500-1166 <sup>2</sup>	200-600 <sup>1</sup>	1750 <sup>2</sup>	357.8 <sup>2</sup>	700-1100 <sup>1</sup>	643-1383 <sup>1</sup>	415-1470 <sup>2</sup>	522-1836 <sup>1,4</sup>

<sup>1</sup>Throughput and energy efficiency were calculated based on a typical convolution layer <sup>3</sup>Area includes only extended units

<sup>2</sup>Throughput and energy efficiency were calculated based on the average values of examined DNNs

<sup>4</sup>GOPs/W for W8I8: 522, W8I4: 546, W8I2: 572, W4I8: 837, W4I4: 1029, W4I2: 1094, W2I8: 1369, W2I4: 1658, W2I2: 1836

highlighting our incremental improvements achieved. We note that our solution is synthesized and evaluated using GlobalFoundries 22nm FDX, an industrial-strength technology, ensuring a more realistic assessment compared to academic PDKs such as the ASAP 7nm library used in our previous work and others. We specifically examine hardware-software co-designed architectures for executing DNNs on CPU-based platforms, incorporating ISA extensions and custom functional units. A detailed comparative analysis is provided in Table V. To assess the performance of our modified RISC-V processor with custom ISA extensions against state-of-the-art solutions, we report the peak performance values stated in each study. For a fair comparison, we consider either a representative convolution layer or the average peak performance across all evaluated DNNs. Some prior works do not account for accuracy degradation in their reported peak performance—sometimes leading to significant trade-offs [3]—and hence, this aspect is not analyzed here. In contrast, our evaluation presents an energy efficiency range with an accuracy deviation of less than 1%, ensuring near floating-point performance.

As presented in Table V, our energy efficiency values correspond to the lowest and highest efficiency achieved across a typical convolution layer, while Table IV presents the efficiency of each examined benchmark. The highest efficiency is observed at 0.62V, the lowest operating voltage where the core design remains within clock constraints. As shown, our lowest energy efficiency, on average (720 GOPs/W), exceeds that of MIX-GEMM [3] when maintaining accuracy degradation below 1%. Compared to [13], our efficiency ranges from  $0.9\times$  up to  $9.2\times$  higher, depending on the configuration. Focusing on MobileNetV1, MIX-GEMM achieves approximately 500 GOPs/W with minor accuracy degradation, whereas our approach surpasses this, reaching 639 GOPs/W and scaling up to 801 GOPs/W with an accuracy loss of up to 5%. Similarly, XPulpNN [5], which integrates SIMD units capable of executing 4 MACs (8-bit) to 16 MACs (2-bit) per cycle, achieves competitive performance on a single convolution layer. However, when evaluated on our full CNN model (1471 GOPs/W), its energy efficiency remains 25% lower than that of our processor. Additionally, UNPU [15], despite its high-

performance decoupled accelerator, faces limitations due to reduced flexibility. The necessity for complex software stacks in such accelerators often demands specialized offloading mechanisms at the hardware or software level, which can impact overall throughput. Note also that when prioritizing energy efficiency over top-1 accuracy, our processor reaches an average of 905 GOPs/W, with a peak performance of nearly 1.8 TOPs/W on the CIFAR10 CNN model under a 5% accuracy degradation. Specifically, the energy efficiency of the best designs satisfying the 2% accuracy loss criteria is 796 GOPs/W averaged across all benchmarks. SPEED [19] achieves a high operating frequency of 1.05 GHz through precise pipeline stage allocation, but this comes at the cost of reduced area and energy efficiency compared to *MaRVIn*. Finally, while our current implementation achieves slightly lower energy efficiency than our previous work [12], due to differences in technology libraries and variations in the power characteristics of the standard cells, it significantly improves raw computational throughput—the prime focus of our work. On average, *MaRVIn* delivers a  $2.5\times$  increase in GOPs compared to its previous version.

## VI. CONCLUSION

In this work, we embrace the power of mixed-precision neural networks to address the limitations of conventional CPU architectures in managing precision efficiently. We propose enhancements in a generic RISC-V CPU core with lightweight hardware modifications and an end-to-end automated framework, *MaRVIn*, for generating and evaluating mixed-precision models. We extend the RISC-V ISA with nine novel instructions, enabling multiple operational modes that optimize computations through operand packing, multi-pumping, and a soft SIMD technique. By integrating these enhancements into a RISC-V-based processor, we demonstrate that accuracy can be maintained while achieving significant improvements in energy efficiency and performance, marking a major step toward energy-efficient computing for resource-constrained devices.

## REFERENCES

- [1] N. P. Jouppi, C. Young, N. Patil, D. Patterson, G. Agrawal, R. Bajwa, S. Bates, S. Bhatia, N. Boden, A. Borchers *et al.*, "In-datacenter performance analysis of a tensor processing unit," in *Proceedings of the 44th annual international symposium on computer architecture*, 2017, pp. 1–12.
- [2] A. Garofalo, M. Rusci, F. Conti, D. Rossi, and L. Benini, "Pulp-nn: A computing library for quantized neural network inference at the edge on risc-v based parallel ultra low power clusters," in *2019 26th IEEE International Conference on Electronics, Circuits and Systems (ICECS)*, 2019, pp. 33–36.
- [3] E. Reggiani, A. Pappalardo, M. Doblas, M. Moreto, M. Olivieri, O. S. Unsal, and A. Cristal, "Mix-gemm: An efficient hw-sw architecture for mixed-precision quantized deep neural networks inference on edge devices," in *2023 IEEE International Symposium on High-Performance Computer Architecture (HPCA)*, 2023, pp. 1085–1098.
- [4] G. Armeniakos, G. Zervakis, D. Soudris, and J. Henkel, "Hardware approximate techniques for deep neural network accelerators: A survey," *ACM Comput. Surv.*, vol. 55, no. 4, nov 2022.
- [5] A. Garofalo, G. Tagliavini, F. Conti, D. Rossi, and L. Benini, "Xpulpnn: Accelerating quantized neural networks on risc-v processors through isa extensions," in *2020 Design, Automation & Test in Europe Conference & Exhibition (DATE)*, 2020, pp. 186–191.
- [6] Y.-H. Chen, T. Krishna, J. S. Emer, and V. Sze, "Eyeriss: An energy-efficient reconfigurable accelerator for deep convolutional neural networks," *IEEE Journal of Solid-State Circuits*, vol. 52, no. 1, pp. 127–138, 2017.
- [7] G. Armeniakos, G. Zervakis, D. Soudris, M. B. Tahoori, and J. Henkel, "Co-design of approximate multilayer perceptron for ultra-resource constrained printed circuits," *IEEE Transactions on Computers*, vol. 72, no. 9, pp. 2717–2725, 2023.
- [8] —, "Cross-layer approximation for printed machine learning circuits," in *2022 Design, Automation & Test in Europe Conference & Exhibition (DATE)*, 2022, pp. 190–195.
- [9] C. Zhou, V. Richard, P. Savarese, Z. Hassman, M. Maire, M. DiBrino, and Y. Li, "Sysmol: A hardware-software co-design framework for ultra-low and fine-grained mixed-precision neural networks," 2023.
- [10] K. Xu, H. Zhang, Y. Li, Y. Zhang, R. Lai, and Y. Liu, "An ultra-low power tinyml system for real-time visual processing at edge," *IEEE Transactions on Circuits and Systems II: Express Briefs*, vol. 70, no. 7, pp. 2640–2644, 2023.
- [11] M. Shafique, R. Hafiz, S. Rehman, W. El-Harouni, and J. Henkel, "Invited: Cross-layer approximate computing: From logic to architectures," in *Design Automation Conference (DAC)*, 2016, pp. 1–6.
- [12] G. Armeniakos, A. Maras, S. Xydis, and D. Soudris, "Mixed-precision neural networks on risc-v cores: Isa extensions for multi-pumped soft neural operations," in *Proceedings of the 43rd IEEE/ACM International Conference on Computer-Aided Design*, 2024, pp. 1–9.
- [13] G. Ottavi, A. Garofalo, G. Tagliavini, F. Conti, L. Benini, and D. Rossi, "A mixed-precision risc-v processor for extreme-edge dnn inference," in *2020 IEEE Computer Society Annual Symposium on VLSI (ISVLSI)*. IEEE, 2020, pp. 512–517.
- [14] N. Bruschi, A. Garofalo, F. Conti, G. Tagliavini, and D. Rossi, "Enabling mixed-precision quantized neural networks in extreme-edge devices," in *Proceedings of the 17th ACM International Conference on Computing Frontiers*, ser. CF '20. New York, NY, USA: Association for Computing Machinery, 2020, p. 217–220. [Online]. Available: <https://doi.org/10.1145/3387902.3394038>
- [15] J. Lee, C. Kim, S. Kang, D. Shin, S. Kim, and H.-J. Yoo, "Unpu: An energy-efficient deep neural network accelerator with fully variable weight bit precision," *IEEE Journal of Solid-State Circuits*, vol. 54, no. 1, pp. 173–185, 2018.
- [16] W. Xu, Z. Zhang, X. You, and C. Zhang, "Reconfigurable and low-complexity accelerator for convolutional and generative networks over finite fields," *IEEE Transactions on Computer-Aided Design of Integrated Circuits and Systems*, vol. 39, no. 12, pp. 4894–4907, 2020.
- [17] S. Wang, X. Wang, Z. Xu, B. Chen, C. Feng, Q. Wang, and T. T. Ye, "Optimizing cnn computation using risc-v custom instruction sets for edge platforms," *IEEE Transactions on Computers*, 2024.
- [18] M. Sun, Z. Li, A. Lu, Y. Li, S.-E. Chang, X. Ma, X. Lin, and Z. Fang, "Film-qnn: Efficient fpga acceleration of deep neural networks with intra-layer, mixed-precision quantization," in *Proceedings of the 2022 ACM/SIGDA International Symposium on Field-Programmable Gate Arrays*, ser. FPGA '22. New York, NY, USA: Association for Computing Machinery, 2022, p. 134–145.
- [19] C. Wang, C. Fang, X. Wu, Z. Wang, and J. Lin, "Speed: A scalable risc-v vector processor enabling efficient multiprecision dnn inference," *IEEE Transactions on Very Large Scale Integration (VLSI) Systems*, vol. 33, no. 1, pp. 207–220, 2025.
- [20] K. Balaskas, A. Karatzas, C. Sad, K. Siozios, I. Anagnostopoulos, G. Zervakis, and J. Henkel, "Hardware-aware dnn compression via diverse pruning and mixed-precision quantization," *IEEE Transactions on Emerging Topics in Computing*, pp. 1–14, 2024.
- [21] L. Lai, N. Suda, and V. Chandra, "Cmsis-nn: Efficient neural network kernels for arm cortex-m cpus," *arXiv preprint arXiv:1801.06601*, 2018.
- [22] B. Jacob and P. Warden, "gemmlowp: A small self-contained low-precision gemm library," <https://github.com/google/gemmlowp>, 2022.
- [23] STMicroelectronics, "X-CUBE-AI - Artificial Intelligence Expansion Package," <https://www.st.com/en/embedded-software/x-cube-ai.html>, 2023.
- [24] A. Burrello, A. Garofalo, N. Bruschi, G. Tagliavini, D. Rossi, and F. Conti, "Dory: Automatic end-to-end deployment of real-world dnns on low-cost iot mcus," *IEEE Transactions on Computers*, vol. 70, no. 8, pp. 1253–1268, 2021.
- [25] J. Lin, W.-M. Chen, Y. Lin, C. Gan, S. Han *et al.*, "Mcnnet: Tiny deep learning on iot devices," *Advances in Neural Information Processing Systems*, vol. 33, pp. 11 711–11 722, 2020.
- [26] A. Capotondi, M. Rusci, M. Fariselli, and L. Benini, "Cmix-nn: Mixed low-precision cnn library for memory-constrained edge devices," *IEEE Transactions on Circuits and Systems II: Express Briefs*, vol. 67, no. 5, pp. 871–875, 2020.
- [27] R. Andri, L. Cavigelli, D. Rossi, and L. Benini, "Yodann: An architecture for ultralow power binary-weight cnn acceleration," *IEEE Transactions on Computer-Aided Design of Integrated Circuits and Systems*, vol. 37, no. 1, pp. 48–60, 2018.
- [28] M. Askarihemmat, S. Wagner, O. Bilaniuk, Y. Hariri, Y. Savaria, and J.-P. David, "Barvinn: Arbitrary precision dnn accelerator controlled by a risc-v cpu," in *Proceedings of the 28th Asia and South Pacific Design Automation Conference*, ser. ASPDAC '23. New York, NY, USA: Association for Computing Machinery, 2023, p. 483–489.
- [29] P. Colangelo, N. Nasiri, E. Nurvitadhi, A. Mishra, M. Margala, and K. Nealis, "Exploration of low numeric precision deep learning inference using intel® fpgas," in *2018 IEEE 26th Annual Int. Symposium on Field-Programmable Custom Computing Machines (FCCM)*, 2018, pp. 73–80.
- [30] V. Leon, M. A. Hanif, G. Armeniakos, X. Jiao, M. Shafique, K. Pekmetstzi, and D. Soudris, "Approximate computing survey, part i: Terminology and software & hardware approximation techniques," *ACM Comput. Surv.*, vol. 57, no. 7, Mar. 2025.
- [31] [www.lowrisc.org](http://www.lowrisc.org), "Ibex risc-v core," <https://github.com/lowRISC/ibex>.
- [32] OpenHW Group, "OpenHW Group CORE-V CV32E40P RISC-V IP," GitHub repository, 2025, <https://github.com/openhwgroup/cv32e40p>.
- [33] Clarie Wolf, "PicoRV32 - A Size-Optimized RISC-V CPU," GitHub repository, 2020, <https://github.com/YosysHQ/picorv32>.
- [34] M. Capra, B. Bussolino, A. Marchisio, G. Masera, M. Martina, and M. Shafique, "Hardware and software optimizations for accelerating deep neural networks: Survey of current trends, challenges, and the road ahead," *IEEE Access*, vol. 8, pp. 225 134–225 180, 2020.
- [35] R. Zhao, T. Todman, W. Luk, and X. Niu, "Deerpump: Multi-pumping deep neural networks," in *2017 IEEE 28th International Conference on Application-specific Systems, Architectures and Processors (ASAP)*, 2017, pp. 206–206.
- [36] W. Snyder, P. Wasson, D. Galbi, and et al, "Verilator," <https://github.com/verilator/verilator>.
- [37] B. Keller, "Risc-v, spike, and the rocket core," *Berkeley Architecture Group*, 2013.
- [38] G. A. Gillani, M. A. Hanif, B. Verstoep, S. H. Gerez, M. Shafique, and A. B. J. Kokkeler, "Macish: Designing approximate mac accelerators with internal-self-healing," *IEEE Access*, vol. 7, pp. 77 142–77 160, 2019.
- [39] A. P. Guerreiro, C. M. Fonseca, and L. Paquete, "The hypervolume indicator: Computational problems and algorithms," *ACM Comput. Surv.*, vol. 54, no. 6, Jul. 2021.
- [40] A. G. Howard, M. Zhu, B. Chen, D. Kalenichenko, W. Wang, T. Weyand, M. Andreetto, and H. Adam, "Mobilenets: Efficient convolutional neural networks for mobile vision applications," *arXiv preprint arXiv:1704.04861*, 2017.
- [41] S. Targ, D. Almeida, and K. Lyman, "Resnet in resnet: Generalizing residual architectures," 2016. [Online]. Available: <https://arxiv.org/abs/1603.08029>
- [42] A. Chowdhery, P. Warden, J. Shlens, A. Howard, and R. Rhodes, "Visual wake words dataset," *arXiv preprint arXiv:1906.05721*, 2019.



**Giorgos Armeniakos** (Member, IEEE) received the Diploma degree from the Department of Electrical and Computer Engineering (ECE), National Technical University of Athens (NTUA), Greece, in 2020, where he is currently pursuing the PhD degree. His research interests include approximate computing, digital circuit design, low power design, machine learning, telecommunications, and optimizations. He has worked as a computer engineer on several research ESA and Horizon projects and has published more than 15 papers. He holds one best paper award

and one best paper nomination for his works on digital approximate designs.



**Alexis Maras** received his Diploma in Electrical and Computer Engineering from the National Technical University of Athens (NTUA) in 2024. He is currently pursuing a PhD at the Microprocessors and Digital Systems Lab (NTUA). His research focuses on software-hardware co-optimization for machine learning applications, with an emphasis on design space exploration for dataflow optimization and the development of efficient hardware accelerators.



**Sotirios Xydīs** (Member, IEEE) received the PhD degree in electrical and computer engineering from the National Technical University of Athens (NTUA), Greece, in 2011. He is currently an assistant professor with the National Technical University of Athens, Department of Electrical and Computer Engineering. His research interests include energy efficient computing, design space exploration, high-level synthesis, accelerator design. He has published more than 100 papers in international journals and conferences and three best paper awards.



**Dimitrios Soudris** (Member, IEEE) received the Diploma and Ph.D. degrees in electrical engineering from the University of Patras, Patras, Greece, in 1987 and 1992, respectively. Since 1995, he has been a Professor with the Department of Electrical and Computer Engineering, Democritus University of Thrace, Xanthi, Greece. He is currently a Professor with the School of Electrical and Computer Engineering, National Technical University of Athens, Athens, Greece. He has authored or coauthored more than 600 papers in international journals/con-

ferences. He has coauthored/coedited seven Kluwer/Springer books. He is also the leader and a principal investigator in research projects funded by Greek Government and Industry, European Commission, ENIAC-JU, and European Space Agency. His current research interests include high performance computing, embedded systems, reconfigurable architectures, reliability, and low-power VLSI design. He was a recipient of the award from INTEL and IBM for EU Project LPGD 25256; ASP-DAC 05 and VLSI 05 awards for EU AMDREL IST-2001-34379, and several HiPEAC awards. He has served as the general/program chair in several conferences.